AIP Advances

Extremely high magnetic-field sensitivity of charge transport in the Mn/SiO_2/*p*-Si hybrid structure

Cite as: AIP Advances **7**, 015206 (2017); https://doi.org/10.1063/1.4974876
Submitted: 01 August 2016 . Accepted: 10 January 2017 . Published Online: 23 January 2017

N. V. Volkov, A. S. Tarasov, D. A. Smolyakov, A. O. Gustaitsev, M. V. Rautskii, A. V. Lukyanenko, M. N. Volochaev, S. N. Varnakov, I. A. Yakovlev, and S. G. Ovchinnikov

COLLECTIONS

Paper published as part of the special topic on Chemical Physics, Energy, Fluids and Plasmas, Materials Science and Mathematical Physics

ARTICLES YOU MAY BE INTERESTED IN

Extremely large magnetoresistance induced by optical irradiation in the Fe/SiO_2/p-Si hybrid structure with Schottky barrier
Journal of Applied Physics **114**, 093903 (2013); https://doi.org/10.1063/1.4819975

The bias-controlled giant magnetoimpedance effect caused by the interface states in a metal-insulator-semiconductor structure with the Schottky barrier
Applied Physics Letters **104**, 222406 (2014); https://doi.org/10.1063/1.4881715

Magnetic-field- and bias-sensitive conductivity of a hybrid Fe/SiO_2/p-Si structure in planar geometry
Journal of Applied Physics **109**, 123924 (2011); https://doi.org/10.1063/1.3600056

© 2017 Author(s).

AIP ADVANCES **7**, 015206 (2017)

Extremely high magnetic-field sensitivity of charge transport in the $Mn/SiO_2/p$-Si hybrid structure

N. V. Volkov,[1] A. S. Tarasov,[1] D. A. Smolyakov,[1,a] A. O. Gustaitsev,[1] M. V. Rautskii,[1] A. V. Lukyanenko,[1] M. N. Volochaev,[1,2] S. N. Varnakov,[1,2] I. A. Yakovlev,[1,2] and S. G. Ovchinnikov[1]
[1]*Kirensky Institute of Physics, Russian Academy of Sciences, Siberian Branch, Krasnoyarsk 660036, Russia*
[2]*Institute of Space Technology, Siberian State Aerospace University, Krasnoyarsk 660014, Russia*

(Received 1 August 2016; accepted 10 January 2017; published online 23 January 2017)

We report on abrupt changes in dc resistance and impedance of a diode with the Schottky barrier based on the $Mn/SiO_2/p$-Si structure in a magnetic field. It was observed that at low temperatures the dc and ac resistances of the device change by a factor of more than 10^6 with an increase in a magnetic field to 200 mT. The strong effect of the magnetic field is observed only above the threshold forward bias across the diode. The ratios between ac and dc magnetoresistances can be tuned from almost zero to 10^8% by varying the bias. To explain the diversity of magnetotransport phenomena observed in the $Mn/SiO_2/p$-Si structure, it is necessary to attract several mechanisms, which possibly work in different regions of the structure. The anomalously strong magnetotransport effects are attributed to the magnetic-field-dependent impact ionization in the bulk of a Si substrate. At the same time, the conditions for this process are specified by structure composition, which, in turn, affects the current through each structure region. The effect of magnetic field attributed to suppression of impact ionization via two mechanisms leads to an increase in the carrier energy required for initiation of impact ionization. The first mechanism is related to displacement of acceptor levels toward higher energies relative to the top of the valence band and the other mechanism is associated with the Lorentz forces affecting carrier trajectories between scatterings events. The estimated contributions of these two mechanisms are similar. The proposed structure is a good candidate for application in CMOS technology-compatible magnetic- and electric-field sensors and switching devices. © *2017 Author(s). All article content, except where otherwise noted, is licensed under a Creative Commons Attribution (CC BY) license (http://creativecommons.org/licenses/by/4.0/).* [http://dx.doi.org/10.1063/1.4974876]

I. INTRODUCTION

Magnetoresistance and magnetoimpedance in various materials and artificial structures attract attention of researches as physical phenomena interesting for both fundamental research and application. The dc and ac magnetoresistive (MR) effects are currently used in magnetic memory cells, sensors, and magnetic antennas.[1] Simple semiconductor magnetoresistive elements can be used in magnetic-field-driven non-volatile reconfigurable logic for implementation of Boolean logic functions,[2] as well as in microwave generators[3] and detectors.[4] Semiconductor structures and devices are of great importance for fundamental research,[5] since any developed magnetoelectronic or spintronic device should be compatible with modern semiconductor electronics. Semiconductor-based MR elements and devices are easy to integrate in semiconductor chips. Thus, semiconductor electronics can acquire new functional capabilities.

[a]E-mail: sda88@iph.krasn.ru

 © Author(s) 2017

Intuitively, one could expect the manifestation of the MR effects in hybrid structures combined from semiconductor and ferromagnetic elements. Indeed, the authors of[6–9] demonstrated spin injection, spin detection, and manipulation by the electron spin states in semiconductor structures with ferromagnetic electrodes of special topology. In other words, the transport properties of these structures can be controlled by a magnetic field. At the same time, it was shown that semiconductor structures without ferromagnetic elements can also exhibit the giant MR effect. Moreover, it was established that the strong MR effect can be implemented simply in the bulk of a semiconductor (e.g., silicon) with a certain doping level at high bias. Several mechanisms were proposed that could be responsible for the strong effect of the magnetic field. The first group of the MR effects is related to inhomogeneous states in semiconductors. In particular, the MR effect in the bulk of silicon is possibly caused by the space charge inhomogeneity.[10] It was assumed that in applied inhomogeneous electric field the electron motion becomes correlated and, consequently, magnetic-field-dependent. The inhomogeneous charge state in the bulk of a semiconductor can be induced by charge injection,[11] which forms regions with the dominant minority and majority carrier conductivity. The external magnetic field bends carrier trajectories at the *n-p* interface between these regions, which results in the strong MR effect.

The second group of the MR effects in semiconductors and semiconductor devices is related to the autocatalytic impact ionization.[12,13] In electric fields above a certain critical value, electrons acquire the energy equal to the ionization energy and generation of electron-hole pairs occurs. This process abruptly enhances the electric current through a device. In magnetic field, electron trajectories are deflected and the impact ionization is suppressed. The magnetoresistance caused by the impact ionization and Lorentz force can be significantly changed by choosing the device topology and experimental geometry. Indeed, the surface or *n-p* interface near current channels of devices can significantly enhance the recombination rate upon deflection of charge trajectories in a magnetic field and, thus, strongly suppress impact ionization and reduce the current.[2,14]

The authors of Refs. 15 and 16 observed the giant ac and dc MR effects in the devices based on metal/insulator/semiconductor (MIS) structures with the Schottky barrier. Different mechanisms of the effect of magnetic field on the transport properties of the devices were proposed. However, it still remains unclear whether the MR effect originates from the bulk of silicon or from the transition region at the Schottky barrier. Our studies on lateral devices and Schottky diodes based on the $Fe/SiO_2/p(n)$-Si hybrid structures showed that the interface states localized in the $SiO_2/p(n)$-Si interfacial region make a significant contribution to magnetotransport.[17–20] These states are involved in recharging and their energy structure is rearranged by a magnetic field. However, this is apparently not the only possible mechanism, since it does not explain the variety of MR effects observed in the MIS-structure-based devices.

Depending on a number of parameters, including topology of a device, temperature, ac or dc current mode, and bias across the structure, the magnetic-field sensitivity is implemented via different mechanisms or their combination. The roles played by the dielectric layer forming a potential barrier, Schottky barrier, and magnetic metal electrode in a hybrid structure remain understudied. The need in fundamental understanding of the mechanisms governing the MR phenomena in hybrid (MIS) structures stimulated us to carry out thorough investigations of the magnetotransport properties of the $Mn/SiO_2/p$-Si structure and compare the results obtained with the data on the structures with a Fe electrode. The dc and ac magnetotransport properties of the manganese-containing structure under low external bias were found to be consistent with those established previously for the $Fe/SiO_2/p$-Si structure. However, as the bias exceeded a certain critical value, the magnetotransport properties drastically changed: the MR attained giant values of about $10^6\%$ in the dc and ac modes in magnetic fields below 0.1 T, which cannot be explained by the mechanisms associated with the interface states in the SiO_2/p-Si interfacial region and attracted by us previously to ground the dc MR and magnetoimpedance. We found that the key role in the giant MR effect under high bias is played by impact ionization.

II. EXPERIMENTAL

$Mn/SiO_2/p$-Si structures were fabricated using the technique developed for fabricating structures with a Fe layer.[17] A *p*-Si(100) wafer with a resistivity of 5 $\Omega \cdot$ cm (a doping density (N_A) of

2×10^{15} cm^{-3}) with the (111) orientation was used as a substrate. The substrate thickness (L) was 350 μm. The substrate surface was precleaned by chemical etching and long-time annealing at temperatures of 400–650°C. Thus, the atomically clean silicon surface was obtained. The process was monitored using high-energy electron backscatter diffraction. Then, the substrate was exposed in the aqueous solution of H_2O_2 and NH_4OH in the ratio 1 : 1 : 1 at 60°C for 30 min. During the exposure, a SiO_2 layer with a thickness of $d \sim 1.5$ nm was formed on the substrate surface. The layer thickness was controlled by spectral ellipsometry. A 15-nm-thick manganese layer was deposited by thermal evaporation at room temperature. The residual pressure in a vacuum chamber was 6.5×10^{-8} Torr and the sputtering rate was 0.25 nm/min. The Mn layer thickness was *in situ* controlled with an LEF-751 high-speed laser ellipsometer. All the fabricated structures were characterized by cross-sectional transmission electron microscopy (TEM). Figure 1a shows a cross-sectional TEM image of the Mn/SiO_2/p-Si interfaces. We would like to emphasize the following features. First, there is no determined SiO_2 layer between silicon and the metal film and, consequently, determined Mn/SiO_2 and SiO_2/p-Si interfaces in the structure with the Fe layer, where the SiO_2 layer in cross-sectional TEM images was not spread.[17] This can be attributed to stronger diffusion of Mn ions in SiO_2 as compared with diffusion of Fe ions. Second, the Mn film is polycrystalline and inhomogeneous over its entire thickness. Two layers can be clearly seen: the lower layer (Mn1) with a thickness of ∼12 nm and the upper layer (Mn2) with a thickness of ∼5 nm. In the current stage of our investigations, we cannot draw any conclusion concerning the difference (crystal structures, morphologies, Si or other impurities, etc.) between these two layers yet. Third, the manganese film surface is coated with a thin (2–3 nm) manganese oxide MnO_x layer, since manganese is oxidized in air.

The magnetic properties of the Mn films were examined using SQUID magnetometry (MPMS-5, Quantum Design) and the magnetooptical Kerr effect (NanoMOKE-2, Quantum Design). According to the data obtained, there is no magnetic order and the manganese film remains paramagnetic even at the lowest temperatures (2 K).

To study the electrical properties of the structure, we fabricated MIS Schottky diodes. The transport properties of a MIS diode in the ac and dc modes were studied in the two-probe configuration. One probe was attached to the top of the Mn electrode with silver epoxy and the other probe, to the substrate backside via an Al-Ga ohmic contact. The contact pad area was 1 mm^2. The device and measuring setup are schematically shown in Fig. 1b. In the dc mode, the resistance and $I-V$ characteristics were measured using a precise KEITHLEY-2400 current/voltage source meter. The $I-V$ characteristics were obtained in the voltage scanning regime. Impedance spectra of the diode were measured with an Agilent E4980A analyzer in the frequency range from 20 Hz to 1 MHz. The ac voltage amplitude was 100 mV. We did not observe the dependence of the impedance spectra on the measuring signal amplitude. The measuring setup allowed us to apply a dc bias (V_b) of up to ±5 V across the device. The magnetotransport properties were investigated in a magnetic field applied in the structure plane.

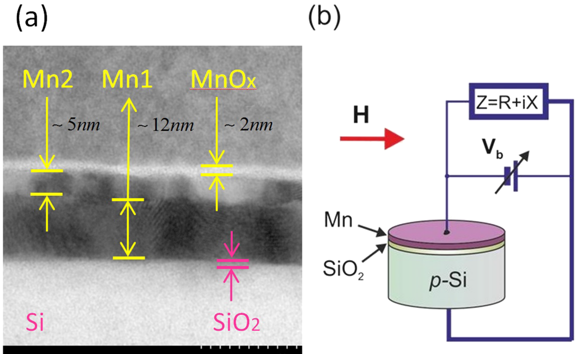

FIG. 1. (a) Cross-sectional TEM images of the Mn/SiO_2/p-Si interfaces. (b) Schematic of the device and measuring setup.

III. RESULTS AND DISCUSSION

A. Magnetoimpedance: Low bias

Study of the magnetotransport properties of the devices based on the Fe/SiO_2/$p(n)$-Si hybrid structures showed that the magnetic field strongly affects only the ac transport properties. In the dc mode, the MR effect is weak even in high magnetic fields of up to 9 T.[17] For this reason, we started studying the Schottky diodes with the Mn electrode with impedance ($Z = R_{ac} + iX$, where R_{ac} and X are the real and imaginary parts of the impedance, respectively) and magnetoimpedance measurements. At reverse and low forward bias V_b ($V_b < V_b^c \approx 2$ V), we obtained the results similar to those reported in[18,20] for the structures with Fe.

At low temperatures ($T < 40$ K), an intense peak is observed in the $R_{ac}(T)$ dependence (the step in $X(T)$). The position and intensity of the peak depend on frequency f of measuring ac voltage V_{ac}. Magnetic field H shifts the peak toward higher temperatures (Fig. 2a). This explains different signs of the MR effect in dependence on f (Figs. 2b and 2c). In this case, the ac MR ratio $MR_{ac} = 100\% \times ((R_{ac}(H) - R_{ac}(0))/R_{ac}(0))$ can attain large values (~200% at $H = 1$ T). The reverse bias affects the peak position in the $R_{ac}(T)$ dependence and, thus, allows the MR_{ac} value to be controlled within a certain range, especially in the low-frequency region, as was observed, e.g., in Ref. 20 for the Fe/SiO_2/n-Si structure. At $V_b < V_b^c$, the forward bias does not noticeably affect the $R_{ac}(T)$ curve.

The special features in the $R_{ac}(T)$ and $X(T)$ dependences are related to the interface states localized in the SiO_2/Si interfacial region and to the processes of their recharging. At a certain temperature, when Fermi level E_F starts crossing energy levels E_S of the interface states, the ac bias V_{ac} across the MIS structure modulates the position of E_S relative to E_F and, thus, initiates capture-emission of electrons from the interface states to the valence band. The peak in the $R_{ac}(T)$

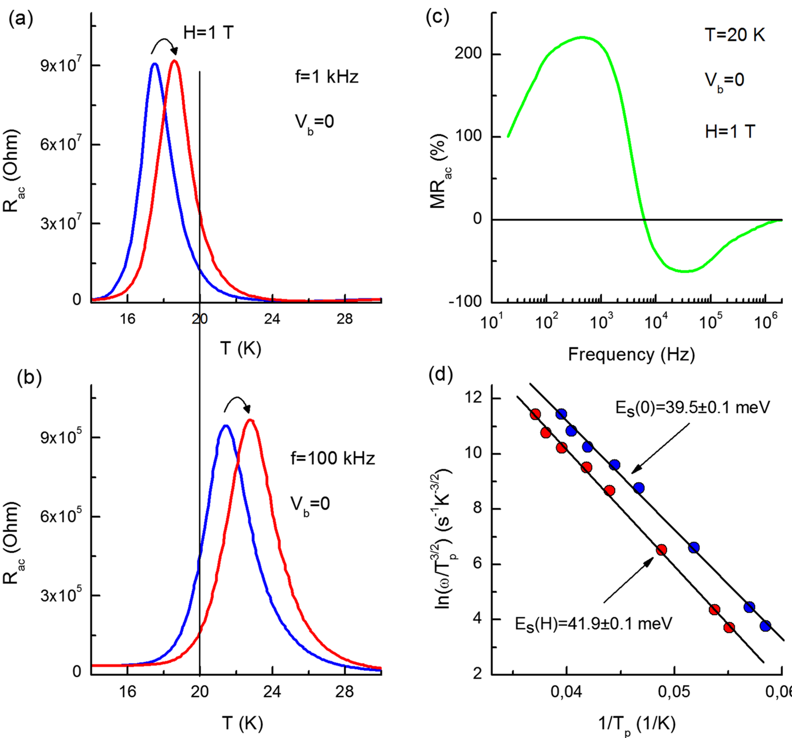

FIG. 2. Temperature dependences of the real part of the impedance at 1 kHz (a) and 100 kHz (b) in zero magnetic field and in a field of 1 T at zero bias. (c) Frequency dependence of ac magnetoresistance at zero bias in a magnetic field of 1 T at temperature of 20 K. (d) Plot of $\ln\left(\omega/T_p^{3/2}\right)$ vs reciprocal peak temperature $1/T_p$ for determining energy levels of the interfacial states in zero magnetic field ($E_S(0)$) and in a field of 1 T ($E_S(H)$).

dependence should occur under the condition $\omega \langle \tau \rangle = 1$, where $\omega = 2\pi f$ is the angular frequency of V_{ac} and $\langle \tau \rangle$ is the average relaxation time, which characterizes the process of charging-discharging of the interface state. The interface states are, in fact, acceptor centers in a p-type semiconductor. The energy levels of acceptor centers are pinned to a certain point in the semiconductor band gap at the SiO_2/Si interface; therefore, upon variation in bias V_b across the MIS structure, the position of the levels at the SiO_2/Si interface changes in accordance with the shift of semiconductor band gap edges. At the same time, the E_F position in the semiconductor remains invariable upon V_b variation.

We can understand the effect of the magnetic field assuming that it shifts the energy levels of interface states (and acceptor levels as a whole) relative to the semiconductor band edges toward higher energies (to the band gap center), as can be seen in Fig. 3a. On the contrary, the bias does not change the distance between E_S and band edges. However, the band bending near the interface between the semiconductor and SiO_2 layer under the action of V_b changes the distance between E_S and E_F (Fig. 3b). The change in the energy state of interface centers under the action of H and V_b can be determined by analyzing the dependences of $\omega/T_p^{3/2}$ on $1/T_p$, where T_p is the peak position in the $R_{ac}(T)$ dependence.[21] When determining the positions of energy levels, we can follow the behavior of coefficient B_T of thermal recombination of a single hole with ionized acceptors. The B_T value is determined from the condition $1/T_p = 0$ (when the curve in Fig. 2d crosses the y axis) and amounts to $9.7 \times 10^{15} m_e^{*3/2} B_T \beta$, where m_e^* is the effective mass and β is the degeneracy.

Analysis of the experimental plots (Fig. 2d) shows that the magnetic field leads to an increase in E_S, while B_T remains almost invariable. This indicates that the field weakly affects such parameters as the capture coefficient, tunneling probability, and densities of states in the metal and semiconductor conduction bands. On the contrary, the bias does not shift E_S, but the variation in B_T is, most likely, due to the change in the capture coefficient and in the probability of carrier tunneling through the SiO_2 potential barrier.

Thus, the mechanisms of the effect of V_b and H on the impedance are generally clear, except for the origin of displacement of the acceptor center energy levels in a magnetic field. Schoonus *et al.*[16] attributed the observed shift to the high-energy region to the fact that the magnetic field shrinks the acceptor wave functions and, thus, leads to a decrease in the overlap of the tales of the functions of neighboring acceptor centers. As a result, the effective energy of acceptor level increases. No physically justified quantitative theory of the effect of the magnetic field on the acceptor levels was built. However, the anisotropy of the magnetic-field response is still unclear. The field perpendicular to the structure plane almost does not affect the positions of special features in the $R_{ac}(T)$ and $X(T)$ curves. At the same time, as we can see, within the proposed mechanism the magnetic field direction should not influence the E_S shift toward higher energies relative to the top of the valence band. As in the previous studies, we pay attention on the relatively large E_s shift in a magnetic field: in a field of 1 T, the shift is more than 2 meV (Zeeman splitting of levels in such fields is no more than 0.06 meV for $S = 1/2$). In this study, we do not answer the question about the origin of the

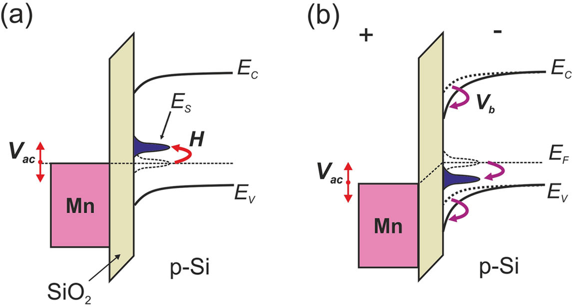

FIG. 3. Schematic band diagram of the Mn/SiO_2/p-Si Schottky diode illustrating the effect of (a) magnetic field and (b) bias on the position of energy levels of the interface states in the band gap.

E_S shift in a magnetic field and discuss only the experimentally proved fact of this shift and experimental values of the E_S variation.

B. Magnetoimpedance: High forward bias

The results discussed above were obtained at $V_b < V_b^c$. At the forward bias above the critical value V_b^c, which, in our case, is about 2 V (this value changes insignificantly with temperature), the behavior of the $R_{ac}(T)$ and $X(T)$ dependences and the effect of the magnetic field on the impedance drastically change. Figure 4a shows that the peak in the $R_{ac}(T)$ curve at low V_b (Fig. 2a) sharply changes its shape, shifts, and decreases in intensity above V_b^c. Already at $V_b > 3$ V, the peak can hardly be seen, while R_{ac} still decreases with increasing V_b. As V_b increases from 0 to 5 V, the R_{ac} value in the peak region decreases by more than five orders of magnitude. In a magnetic field, the initial peak size and shape rapidly recover. Already at 250 mT, the peak intensity coincides with that at $V_b = 0$, but with a further increase in H, a small shift of the peak to the high-temperature region is observed (Fig. 4b). Figure 4c shows the behavior of R_{ac} as a function of H at fixed temperature for $V_b = 0$ and $V_b = 5$ V. The response to the magnetic field strongly changes under the bias; the magnetoresistance ratio increases from 200 to 10^5%; the largest changes in R_{ac} are observed in relatively weak fields ($H < 250$ mT). It can be seen in Fig. 4d that the magnetoresistance ratio sharply increases only at forward biases above V_b^c. All the data presented in Fig. 4 were obtained at a measuring voltage frequency of 1 kHz.

Figure 5 presents frequency dependences of R_{ac} in different magnetic fields and the corresponding dependences of MR_{ac} at $V_b > V_b^c$. In contrast to the case $V_b < V_b^c$ (Fig. 2c), at high bias, already around 1 MHz, the device exhibits a fairly high positive MR ($MR_{ac} > 10^3$%), which rapidly grows with a decrease in frequency to about 5 kHz. Then, the growth slows down, but, in contrast to the low-bias case, continues up to the lowest frequencies and the values $MR_{ac} > 10^7$% are attained.

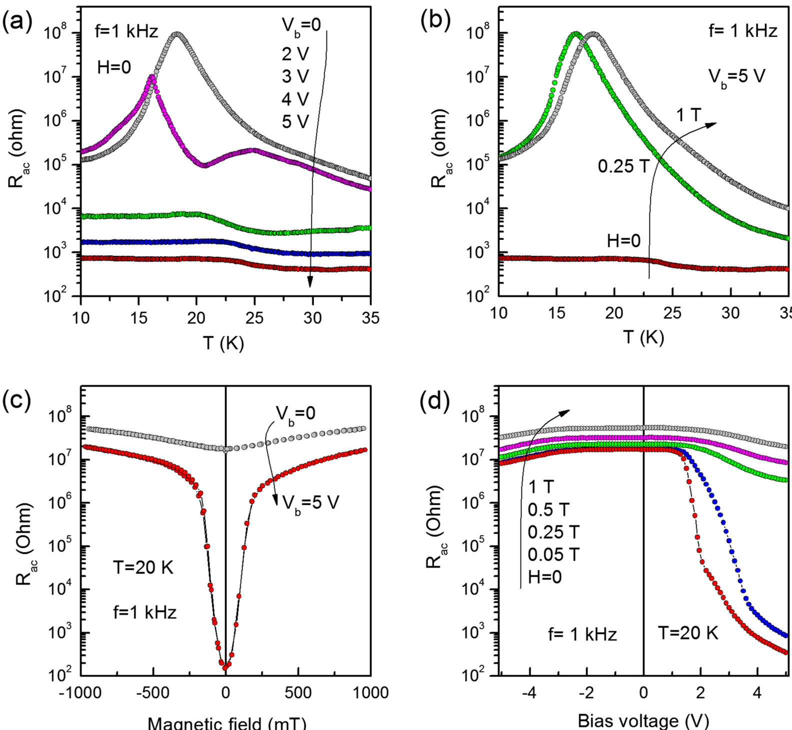

FIG. 4. Real part of the impedance (a) as a function of temperature for forward biases from zero to 5 V without magnetic field, (b) as a function of temperature for magnetic fields from zero to 1 T at a forward bias of 5 V, (c) as a function of magnetic field for zero bias and a forward bias of 5 V, and (d) as a function of bias voltage for magnetic fields from zero to 1 T at T = 20 K. The frequency is 1 kHz.

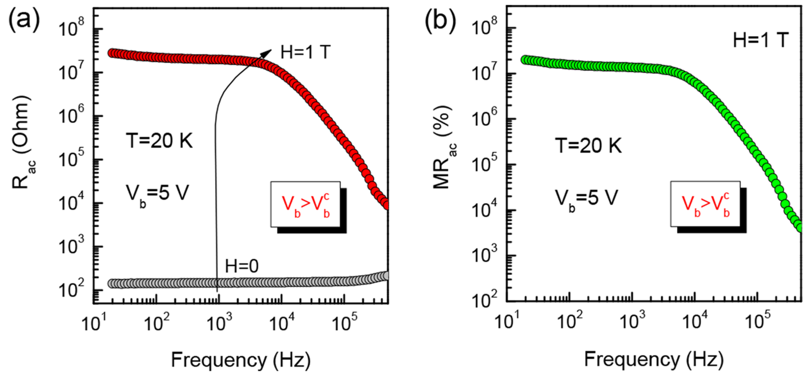

FIG. 5. Frequency dependences of (a) the real part of ac resistance without magnetic field and in a field of 1 T and (b) ac magnetoresistance in a magnetic field of 1 T. The forward bias is 5 V and the temperature is 20 K.

C. The dc magnetoresistive effect

Since at $V_b > V_b^c$ we observe the largest MR_{ac} values at the lowest frequencies, it is reasonable to investigate the MR effect in the dc mode and its dependence on V_b. Recall that in the $Fe/SiO_2/p(n)$-Si structures,[17] the dc MR value (MR_{dc}) was lower than 20% in a field of 9 T. In the $Mn/SiO_2/p$-Si structure, the MR effect is also insignificant at $V_b < V_b^c$, but, as can be seen in Fig. 6a, in the low-temperature region at $V_b > V_b^c$ the MR_{dc} value exceed 10^7%. The strongest changes in the R_{dc} value are observed in even weaker fields (H<100 mT) than in the ac mode (Fig. 4c).

As expected, the $I-V$ characteristics are nonlinear. In the temperature range of 40–300 K, they are typical of a MIS diode with the Schottky barrier and weakly change with temperature (Fig. 7a). This confirms that in this temperature range the physical mechanisms of carrier transport remain invariable. It can be seen in Fig. 7b that below 40 K the $I-V$ characteristics become more complex and magnetic-field-sensitive. This can indicate switching of additional conductivity mechanisms in the structure at low temperatures. In zero magnetic field, the current through the diode under forward bias attaining the threshold value $V_b^c \approx 2$ V increases by several orders of magnitude. As can be seen in Figs. 7c and 7d, the effect of the magnetic field is reduced to shifting the threshold voltage at which the feature in the $I-V$ characteristics is observed. The V_b^c value rapidly grows with field and the slope of the $I-V$ curves above V_b^c remains almost invariable.

Let us now consider the main mechanisms that determine the special features of current flow through the diode. When the voltage is applied to the diode, the potential drop occurs on the Schottky barrier (V_{Sch}) formed at the Si/SiO_2 interface, in the dielectric SiO_2 layer (V_i), and in the bulk of the

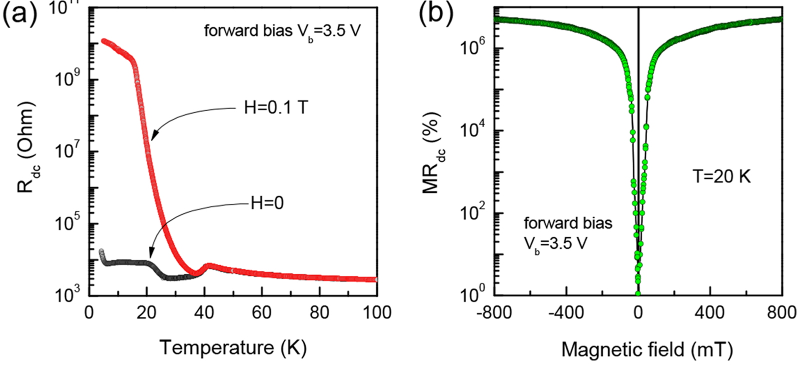

FIG. 6. (a) Temperature dependences of dc resistance at a forward bias of 3.5 V without magnetic field and in a field of 0.1 T. (b) Dc magnetoresistance ratio as a function of magnetic field at a temperature of 20 K and a forward bias of 3.5 V.

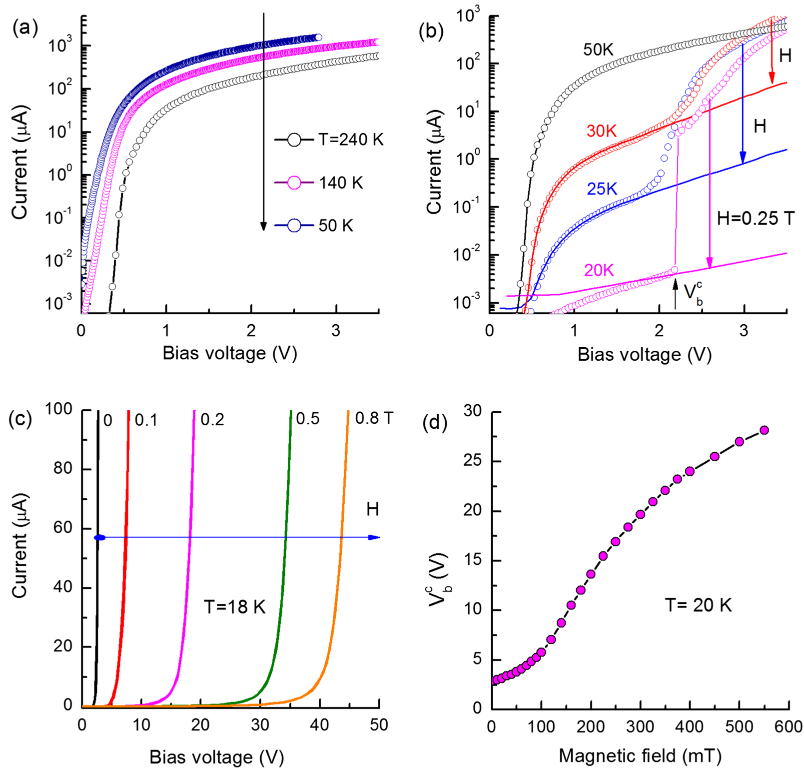

FIG. 7. I–V curves (a) at $H = 0$ and different temperatures above 50 K, (b) at $H = 0$ (open circles) and $H = 0.25$ T (solid lines) at different temperatures below 50 K, and (c) in magnetic fields of up to 0.8 T at 18 K. (d) Threshold voltage (V_b^c) as a function of magnetic field at 20 K.

Si substrate (V_{Si}). Thus, the total voltage across the diode can be written as

$$V_{tot} = V_{Sch} + V_i + V_{Si} \tag{1}$$

The behavior of the I–V characteristics in the temperature range of 50–300 K (Fig. 7a) suggests that here the key role is apparently played by the Schottky barrier. The density of current flowing through the Schottky barrier[22] is determined by thermionic emission and can be written in the form

$$J = A^* T^2 e^{-q\phi/k_B T} \left(e^{qV_{Sch}/\eta k_B T} - 1 \right) \tag{2}$$

where A^* is the effective Richardson constant, ϕ is the Schottky barrier height, and η is the ideality factor of the barrier, which is usually close to unity, so in the further estimations we use the value $\eta = 1$. However, the experimental I–V characteristics are not satisfactorily approximated by Eq. (2). The discrepancy between the experiment and calculation is especially large at high biases. Therefore, we are forced to take into account other possible contributions.

One of these contributions is associated with the SiO_2 layer and defects formed in it. Here, we assume that such defects can be formed by Mn atoms, which, as we mentioned above, can diffuse in the silicon oxide layer with high probability. A thin dielectric layer with defects obeys the Ohm′s law at low voltages and the quadratic voltage dependence of current at high voltages. Defects form trap energy levels.[23] At high voltages, carriers acquire the energy sufficient to be captured by these traps, which induces the space charge. As a result, the current through the dielectric becomes space-charge-limited and obeys the well-known Mott–Gurney law

$$J = \frac{9\varepsilon\mu V_i^2}{8\theta d^3}. \tag{3}$$

Here, ε is the permittivity of the dielectric layer, μ is the carrier mobility, d is the SiO_2 layer thickness, and θ is the ratio between the number of carriers captured by the traps and the total

number of injected carriers. In the simplest case of traps with the only energy level, which have density N_t and are distant from the conduction band by E_t, this ratio is approximately

$$\theta = \frac{N_C}{N_t} \exp\left(-\frac{E_t}{k_B T}\right), \tag{4}$$

where N_C is the number of states in the bottom slice $k_B T$ of the conduction band. Below, we use this expression to approximate the $I-V$ characteristics, being aware of the fact that in the investigated structure the traps should be widely distributed by energy, and, consequently, the behavior of ratio θ upon temperature and voltage variation is more complex.[24]

Regarding the formation of defects in the structures similar to that investigated here, it is caused by the amorphous state of SiO_2 and strong diffusion of 3d ions in SiO_2 and Si. In our case, the absence of a clearly determined SiO_2 layer in cross-sectional TEM images of the Mn/SiO_2/*p*-Si interfaces (see Section II) can also be indicative of strong diffusion of Mn ions and, consequently, of the large number of defects in the dielectric layer.

It should be noted that dependence (3) can also be implemented in semiconductors with the localized trapping states.[10,23] In the investigated structure, we can expect such a behavior for the *p*-type semiconductor, but only at low temperatures, when the acceptor states capture holes and can serve as trapping states for electrons injected into the semiconductor. However, since the behavior of the $I-V$ characteristics with the typical quadratic contribution (Eq. (3)) is observed at high temperatures, it cannot originate from the bulk of silicon.

Finally, the $I-V$ characteristic of the structure will contain the contribution from the current flowing through the Si substrate. At high temperatures for any bias and at low temperatures for low bias ($V_b < V_b^c$), we may assume that the current through the bulk of the semiconductor is ohmic, i.e., $V_{Si}=I \times R_{Si}$. The temperature dependence of resistance R_{Si} is determined mainly by the temperature dependence of carrier density n(the density of holes in *p*-Si), because $R_{Si} = L\Big/\left(S_{eff} \cdot n\mu q\right)$, where L is the Si substrate thickness, S_{eff} is the active area of the junction, and μ is the charge mobility, which weakly changes with temperature. The temperature dependence of n is

$$n(T) = \left(\frac{N_A N_V(T)}{2}\right)^{1/2} \exp\left(-\frac{E_A}{2k_B T}\right), \tag{5}$$

taking into account that the effective density of states in the valence band is calculated as

$$N_V(T) = 2 \cdot \left(\frac{2\pi m_e k_B T}{h^2}\right)^{3/2}, \tag{6}$$

where N_A is the acceptor concentration and E_A is the position of the acceptor impurity energy levels in the semiconductor band gap (coincides with E_S).

Finally, the relation between the bias and current for the structure under study can be written as

$$V_{tot} = \left[\frac{k_B T}{q} \ln\left(\frac{I}{S_{eff} J_0} + 1\right)\right]_{Sch} + \left[\sqrt{\frac{8Id^3\theta}{9S_{eff}\varepsilon\mu}}\right]_i + \left[\frac{IL}{S_{eff} \cdot n(T)\mu q}\right]_{Si}, \tag{7}$$

where $J_0 = A^* T^2 \exp(-q\phi/k_B T)$.

Thus, the main features of the $I-V$ characteristics, except for the case of high bias at low temperatures, can be interpreted as follows. At low bias, the largest contribution to the structure resistance is made by the Schottky barrier. As V_b increases, the barrier resistance decreases, while the dielectric layer resistance starts growing. It is the amorphous SiO_2 layer with numerous defects that limits the growth of the current through the structure at high bias and determines the functional dependence $I(V_b)$ in accordance with the Mott–Gurney law.

Figure 8a presents an example of approximation of the experimental $I-V$ characteristic at $T = 50$ K using expression (7) with the parameters that are quite realistic for our structure: $\phi = 0.4$ eV, $\varepsilon = 3.5 \cdot 10^{-13}$ F/cm, $\mu = 10^3$ cm^{2}V^{-1}s^{-1}, $N_C = 10^{19}$, $N_t = 10^{17}$, and $E_t = 0.14$ eV. The other parameters were given above. The approach used explains the strong temperature dependence of the $I-V$ characteristics below 40 K (Fig. 8b). We changed only temperature; all the rest parameters

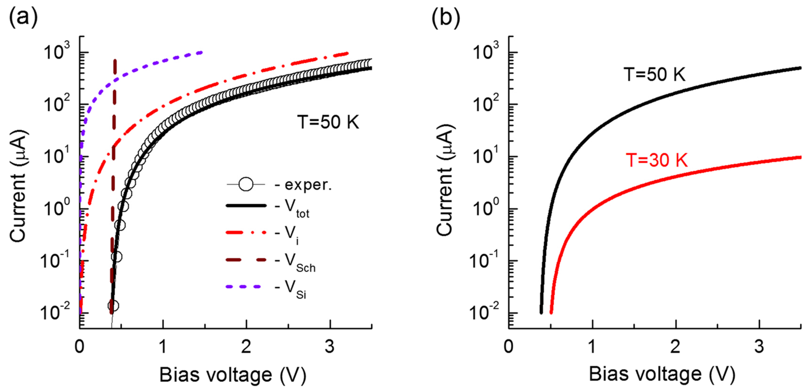

FIG. 8. (a) $I-V$ characteristics of the diode. Symbols show experimental results for the diode at 50 K; solid lines, data calculated using expression (7); and dash-and-dot, dashed, and dotted lines, calculated contributions of the SiO_2 layer, Schottky barrier, and Si substrate, respectively, to the $I-V$ characteristics. (b) $I-V$ characteristics at temperatures of 50 and 30 K.

were fixed. Certainly, we could hardly expect better quantitative agreement, since the structure under study is imperfect and Eqs. (2–7) were written with serious assumptions. Nevertheless, the main parameter determining the behavior of the transport properties at temperatures of $T < 40$ K is obviously hole density n in the bulk of the Si substrate. Around 40 K, E_F becomes lower than E_A and the acceptor states start intensively trapping holes. The majority carrier density starts decreasing with temperature (Eq. (5)), which leads to a sharp decrease in the current through the structure.

Let us now consider the special feature that arises in the $I-V$ characteristics below 40 K at V_b^c. There is good reason to believe that the sharp growth of the current above the threshold voltage and the main features in the transport properties at $V_b > V_b^c$ are related to autocatalytic impact ionization of shallow acceptor boron in the bulk of the semiconductor. When the high bias voltage is applied, carriers acquire the kinetic energy that exceeds the energy of ionization of acceptor impurities; i.e., impact ionization occurs. Since the ionization energy ($\sim E_A$) is only about 40 meV, the breakdown occurs already in fields of few V/cm and lasts until all impurities are ionized. The measured time dependences of the current at pulsed voltage switching above V_b^c are exponential, i.e., typical of impact ionization. The change in the device current with time and the breakdown criterion can be quantitatively estimated using the balance equation for a kinetic process, which determines the hole density in a certain electric field (at a certain bias voltage).[25] In the simplified case, this equation can be written in the form

$$\frac{dn}{dt} = -\frac{(n - n_0)}{\tau}, \tag{8}$$

which yields the exponential time dependence. Here, n_0 is the static hole density and τ is the time constant. The both quantities are functions of the coefficient of thermal recombination of a hole with ionized acceptors (B_T) and of the coefficients of thermal (A_T) and impact (A_I) ionization. The breakdown occurs in the electric field with strength F_B (under the assumption of electric field homogeneity, $F_B \sim V_b^c$), when the condition

$$B_T\,(F_B)\,N_D - A_I\,(F_B)\,(N_A - N_D) = 0, \tag{9}$$

is satisfied. Here, N_A and N_D are the acceptor and donor concentrations, respectively. Well before the breakdown, we have $A_I << B_T$; with an increase in F in the breakdown region, A_I starts rapidly growing, while B_T changes insignificantly. In this case, A_I exponentially depends on the acceptor level depth ($A_I \sim \exp(-E_A/(k_B T))$, which, in fact, suggests the exponential dependence of F_B on E_A.[25]

As we showed above when studying the structure impedance, in a magnetic field the E_A value shifts to the high-energy region by ΔE_A^H. Qualitatively, it is obvious that the enhancement of E_A

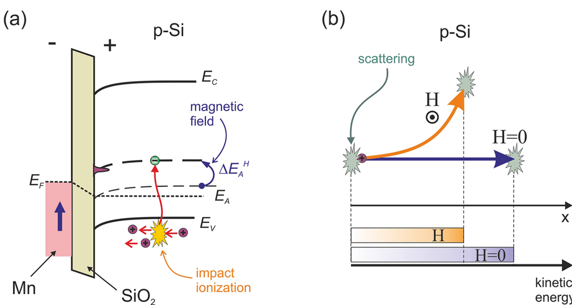

FIG. 9. Schematic diagrams illustrating the effect of the magnetic field on impact ionization. (a) Shift of acceptor levels increases the impact ionization activation energy. (b) Deflection of a carrier trajectory in the magnetic field suppresses acquisition of the kinetic energy between scattering events.

relative to the valence band results in the growth of the impact ionization activation energy; i.e., the process will be initiated at large F_B (V_b^c) (Fig. 9a). Taking into account that, in our case, E_A is about 40 meV and ΔE_A^H is merely about 2 meV in a magnetic field of 1 T, the A_I value will change by a factor of about 3. One should expect that the variation in V_b^c will not exceed this value, which, however, is much less than the experimentally obtained factor 20. Obviously, it is necessary to attract other mechanisms of the effect of the magnetic field.

We can expect the carrier mobility to decrease with increasing magnetic field.[26] The magnetic field can affect tunneling processes resulting from electric-field redistribution in the structure.[27] For both investigated mechanisms, the strong effect of the magnetic field can hardly be expected.

In recent time, the mechanisms associated with the Lorenz force have been actively discussed in the literature.[2,12–14] In applied magnetic field, the Lorentz force deflects carrier trajectories, which increases the probability of inelastic scattering, decreases the kinetic energy of carriers, and, as result, suppresses impact ionization (Fig. 9b). To restore the impact ionization process, stronger electric fields are required. In order words, the magnetic field increases the threshold voltage of the current breakdown.[28] In the classical consideration, under the assumption of parabolic band dispersion in the system, in the weak magnetic field approximation, we can obtain the quadratic dependence of F_B (V_b^c) on H:[29]

$$\frac{V_b^c(H)}{V_b^c(0)} = 1 + \alpha H^2 \tag{10}$$

where $V_b^c(H)$ and $V_b^c(0)$ are the threshold voltages in nonzero and zero magnetic fields, respectively, and α is the parameter depending on the position of acceptor levels, carrier effective mass and mobility, and some other physical quantities. Simple estimations show that the described Lorentz force-related mechanism explains well the experimentally observed growth of V_b^c in a magnetic field. In this case, the initial portion of the experimental $V_b^c(H)$ curve is, indeed, the quadratic dependence. In strong magnetic fields, the nature of deflection is obvious: the approximations and simplifications used by us in deriving Eq. (10) stop working. In the framework of the investigated mechanism, the anisotropy of the effect of the magnetic field becomes clear: the transport properties change most in a magnetic field perpendicular to the current, whereas in a magnetic field parallel to the current, the transport properties are negligibly affected by the field.

We cannot explain the role played by the dielectric barrier, Schottky barrier, and metal electrode material yet. Meanwhile, judging by the data obtained by us and other authors, this item is of principle importance. To date, we can only state that they assist autocatalytic impact ionization and determine the conditions for its triggering.

IV. CONCLUSIONS

It was shown that the ac and dc transport properties of the Schottky diode based on the Mn/SiO$_2$/*p*-Si structure are highly sensitive to external magnetic fields at low temperatures. For

both the dc resistance and the impedance of the device, we can distinguish several regimes of the response to the magnetic field. The dc MR effect, negligible under reverse or low forward bias, rapidly increases and attains huge values at high voltages. The giant MR effect originates from impact ionization initiated in the bulk of the Si substrate when the bias voltage attains a threshold value. The effect of the magnetic field is reduced to suppression of impact ionization, which strongly changes the $I-V$ characteristics and results in the huge (up to 10^8%) magnetoresistance ratio. Impact ionization is suppressed via the two mechanisms whose contributions are of the same order of magnitude. The first mechanism is displacement of the acceptor levels toward higher energies relative to the top of the valence band of the semiconductor, which requires higher voltages to initiate impact ionization. The second mechanism is related to the Lorentz force: deflection of carrier trajectories in a magnetic field suppresses acquisition of the kinetic energy between scattering events; therefore, impact ionization starts at higher bias voltages.

In the case of magnetoimpedance, only the interface states formed in the SiO_2/Si interfacial region work. Similar to the acceptor levels, the surface state levels shift to the high-energy region in a magnetic field, which affects their recharging and, consequently, leads to the impedance variation. The ac MR ratio attains fairly high values of up to 200%. The strong effect of bias on the magnetoimpedance is observed only at the voltages of impact ionization in the bulk of the semiconductor. This results from full ionization of both the acceptor levels in Si and interface states, which completely suppresses recharging of the latter and leads to the abrupt impedance drop. Suppression of impact ionization by a magnetic field rapidly recovers high impedance values and, thus, leads to the large magnetoimpedance ratio (up to 10^6%).

We believe that the discussed mechanisms of giant magnetotransport phenomena can be used to design novel CMOS technology-compatible magnetoresistive devices. Moreover, using the standard CMOS technology with manganese as a metal layer, one can create high sensitive ac and dc detectors of magnetic field.

ACKNOWLEDGMENTS

The reported study was funded by Russian Foundation for Basic Research, Government of Krasnoyarsk Territory, Krasnoyarsk Region Science and Technology Support Fund to the research Projects Nos. 16-42-242036 and 16-42-243046, the Russian Ministry of Education and Science, state assignment no. 16.663.2014K.

[1] A. Fert, Phys. Usp. **51**, 1336 (2008).
[2] S. Joo, T. Kim, S. H. Shin, J. Y. Lim, J. Hong, J. D. Song, J. Chang, H.-W. Lee, K. Rhie, S. H. Han, K.-H. Shin, and M. Johnson, Nature **494**, 72–76 (2013).
[3] S. I. Kiselev *et al.*, Nature (London) **425**, 380 (2003).
[4] Y. Suzuki and H. Kubota, J. Phys. Soc. Jpn. **77**, 031002 (2008).
[5] R. Jansen, Nature Materials **11**, 400 (2011).
[6] Y. Ando, K. Hamaya, K. Kasahara, Y. Kishi, K. Ueda, K. Sawano, T. Sadoh, and M. Miyao, Appl. Phys. Lett. **94**, 182105 (2009).
[7] Y. Ando, Y. Maeda, K. Kasahara, S. Yamada, K. Masaki, Y. Hoshi, K. Sawano, K. Izunome, A. Sakai, M. Miyao, and K. Hamaya, Appl. Phys. Lett. **99**, 132511 (2011).
[8] S. Takahashi and S. Maekawa, Sci. Technol. Adv. Mater. **9**, 014105 (2008).
[9] S. P. Dash, S. Sharma, R. S. Patel, M. P. de Jong, and R. Jansen, Nature (London) **462**, 491 (2009).
[10] M. Delmo, S. Yamamoto, S. Kasai, T. Ono, and K. Kobayashi, Nature (London) **457**, 1112 (2009).
[11] C. Wan, X. Zhang, X. Gao, J. Wang, and X. Tan, Nature (London) **477**, 304 (2011).
[12] J. Lee, S. Joo, T. Kim, K. H. Kim, K. Rhie, J. Hong, and K.-H. Shin, Appl. Phys. Lett. **97**, 253505 (2010).
[13] J. J. H. M. Schoonus, P. P. J. Haazen, H. J. M. Swagten, and B. Koopmans, J. Phys. D: Appl. Phys. **42**, 185011 (2009).
[14] C. Ciccarelli, B. G. Park, S. Ogawa, A. J. Ferguson, and J. Wunderlich, Appl. Phys. Lett. **97**, 082106 (2010).
[15] Z. G. Sun, M. Mizuguchi, T. Manago, and H. Akinaga, Appl. Phys. Lett. **85**, 5643 (2004).
[16] J. J. H. M. Schoonus, F. L. Bloom, W. Wagemans, H. J. M. Swagten, and B. Koopmans, Phys. Rev. Lett. **100**, 127202 (2008).
[17] N. V. Volkov, A. S. Tarasov, E. V. Eremin, S. N. Varnakov, S. G. Ovchinnikov, and S. M. Zharkov, J. Appl. Phys. **109**, 123924 (2011).
[18] N. V. Volkov, A. S. Tarasov, E. V. Eremin, A. V. Eremin, S. N. Varnakov, and S. G. Ovchinnikov, J. Appl. Phys. **112**, 123906 (2012).
[19] N. V. Volkov, A. S. Tarasov, E. V. Eremin, F. A. Baron, S. N. Varnakov, and S. G. Ovchinnikov, J. Appl. Phys. **114**, 093903 (2013).
[20] N. V. Volkov, A. S. Tarasov, D. A. Smolyakov, A. O. Gustaitsev, V. V. Balashev, and V. V. Korobtsov. Appl. Phys. Lett. **104**, 222406 (2014).

[21] D. L. Losee, J. Appl. Phys. **46**, 2204 (1975).
[22] S. M. Sze, *Semiconductor Devices* (Wiley, New York, 1985).
[23] M. A. Lampert, Phys. Rev. **103**, 1648–1656 (1956).
[24] A. Rose, Phys. Rev. **97**(6), 1538 (1955).
[25] M. E. Cohen and P. T. Landsberg, Phys. Rev. **154**(3), 683 (1967).
[26] R. J. Sladek, J. Phys. Chem. Solids **5**, 157 (1958).
[27] L. Y. L. Shen and J. M. Rowell, Phys. Rev. **165**(2), 566 (1968).
[28] S. Salahuddin, Nature **494**, 43 (2013).
[29] J. Hong *et al.*, preprint arXiv:1206.1094v1 (2012).